The potential of Meudon spectroheliograph for investigating long term solar activity and variability

Jean-Marie Malherbe, Isabelle Bualé, Daniel Crussaire, Florence Cornu, Thierry Corbard

Available online at www.sciencedirect.com

ScienceDirect

Advances in Space Research xx (2022) xxx-xxx

The potential of Meudon spectroheliograph for investigating long term solar activity and variability

Jean-Marie Malherbe[a], Isabelle Bualé[a], Daniel Crussaire[a], Florence Cornu[a], Thierry Corbard[b]

[a]*Observatoire de Paris, PSL Research University, CNRS, LESIA, 92195 Meudon, France*
[b]*Université de la Côte d'Azur, Observatoire de la Côte d'Azur, CNRS, Lagrange, 06004 Nice, France*

Received 5 February 2022; Received in final form -; Accepted -;
Available online -

Abstract

Observations of the chromosphere with Deslandres's spectroheliograph started at Paris Observatory in 1893 and were followed by systematic observations at Meudon since 1908. The solar collection of Hα and CaII K images is probably the longest available worldwide, with associated products such as synoptic maps and tables. Since 2018, Meudon spectroheliograph is the only instrument producing data-cubes of full line profiles of CaII H, CaII K and Hα, for each pixel of the solar disk. Slices of the cubes provide monochromatic images. We summarize in this paper the capabilities of the successive generations of the instrument, and explore the potential of the collection and products for analysis of rare events, investigations of past solar activity and studies of long term variability.

Keywords: Instrumentation ; Spectroscopy ; Solar Chromosphere ; Solar Activity ; Solar Variability ; Long Term Observations ; Space Weather

1. Introduction

Solar activity is the primary driver of space weather phenomena, such as flares, eruptive filaments or prominences and coronal mass ejections (CMEs). Observations and models of CMEs are reviewed by Webb & Howard (2012) and Chen (2011), while solar perspectives of space weather are presented in details by Schwenn (2006) and revisited by Temmer (2021). The physics of flare productive active regions (ARs) is investigated by Toriumi & Wang (2019). The magnetic energy stored in ARs, composed of sunspot groups, photospheric faculae or chromospheric plages, plays a major role. When the magnetic topology evolves and becomes unstable, a part is converted into thermal and kinetic energy. The 11-year cycle and its modulations (such as the more or less centennial Gleissberg cycle), reviewed by Hathaway (2010), are the manifestation of solar activity in terms of sunspot number, facular area, magnetic field inversions and irradiance fluctuations. Ground based instruments observe the photosphere and the chromosphere at the source of solar activity, and form networks, such as the GONG (Harvey et al., 2011) or the Global Hα Network (GHN, Steinegger et al. (2000)). Some institutes, such as Meudon, Mount Wilson or Kodaikanal, started systematic observations at the beginning of the twentieth century and have exceptional collections of monochromatic images. In EUV, daily observations of the low and hot corona began with SOHO/EIT (ESA/NASA) in 1996, STEREO/SECCHI (NASA) in 2006 and continue with SDO/AIA (NASA) since 2010. In radio wavelengths, the solar survey is made by radio-heliographs, such as those of Nançay or Nobeyama. Wide field images of the solar environment are also obtained in white light by LASCO coronagraphs (C2 and C3) onboard SOHO, and allow to monitor the progression of solar events at large distance (up to 30 solar radii).

Email addresses: Jean-Marie.Malherbe@obspm.fr (Jean-Marie Malherbe), Isabelle.Buale@obspm.fr (Isabelle Bualé), Daniel.Crussaire@obspm.fr (Daniel Crussaire), Florence.Cornu@obspm.fr (Florence Cornu), Thierry.corbard@oca.eu (Thierry Corbard)

Ground based observatories provide either long-term, low cadence, or short-term, high cadence observations. The former often use spectroheliographs since one century or more, the latter Fabry-Pérot or Lyot filters. The International Geophysical Year (IGY, 1957) was the starter of the monitoring of solar events at high cadence. While filters allowed to study the chronology and details of fast evolving events, such as flares and eruptive prominences, spectroheliographs produced extended collections covering up to 10 cycles, which are useful to investigate rare events of solar activity, or rebuild past irradiance or magnetism via proxies. Long series of observations have been collected at Mount Wilson (Lefebvre et al., 2005), Kodaikanal (Chatzistergos et al., 2019), Arcetri (Ermolli et al., 2009), Mitaka (Hanaoka, 2013) or Coimbra (Lourenço et al., 2019). CaII K collections of these institutes respectively began in 1915, 1904, 1931, 1917 and 1925. Most of them stopped systematic observations with spectroheliographs, apart Meudon and Coimbra (both instruments have similar characteristics). Daily observations started at Meudon in 1908 with images of the chromosphere in CaII K3 (line centre) and Hα, and of the photosphere in CaII K1v (blue wing). Observations continue today with outstanding performance (data-cubes of line profiles of CaII H, K and Hα).

Much before the birth of fast cadence instruments using filters, the visual spectrohelioscope was invented by Hale (1929b) for monochromatic motion picture. It is based on the principles enounced earlier by Janssen in 1869 (memories by Deherain (1929), pages 185 and 198). Later, a spectroheliokinematograph was built at Kitt Peak by McMath & Petrie (1934) using a 35 mm motion picture camera (McMath et al., 1932). It was followed soon by the invention of the birefringent filter (Lyot, 1944) much more convenient for high cadence photographic imagery.

This paper presents the evolutions of Meudon spectroheliograph and the exceptional collection spanning 10 solar cycles (1908-2022). Section 2 summarizes the history and principles of the spectroheliograph, while Section 3 presents derived products, such as synoptic maps and tables of solar activity. Section 4 shows some examples of rare event observations that can be studied with the collection, while the capabilities of the new 2018 version are reported in Section 5.

2. Historical background of the spectroheliograph

The spectroheliograph was invented at the same time, but independently, by Hale (1907) and Deslandres (1908), following Janssen's initial idea, presented at the french Academy of Sciences in 1869, concerning prominence observations. In France, the first instruments were installed in Paris and sporadic observations in CaII K line started in 1893. Deslandres moved to Meudon in 1898 and put his instruments on an inclined and rolling table fed by a small polar siderostat. Many changes and experiments occured until 1907, when a much larger quadruple spectroheliograph, described by D'Azambuja (1920b) and D'Azambuja (1920a) was finally built in a new laboratory; it was fed by a coelostat with two 50 cm mirrors. Figure B.1 shows the entrance objective (part 1, 250 mm aperture, f = 4 m, F/16) which delivers an image of 37.2 mm diameter; it moves slowly (20 s to several minutes) to scan the Sun by the spectrograph slit (30 μm or 1.5 arcsec, part 2). Until 2001, the magnification of the spectrograph was 2.3. In the focal plane, a second slit (part 3) selected the spectral line. The dispersive element was a plane grating for Hα (order 4) and three prisms for CaII K until 1988, with two independent chambers (A1 and A2). Both lines used after this date the same and new blazed grating, and chamber (A1). The bandwidth was 0.25 Å and 0.15 Å, respectively for Hα (order 5) and CaII K lines (order 3). The output image had a diameter of 86 mm and was formed on a 13 x 18 cm^2 photographic plate (glass or film) which translated in perfect synchronism with the entrance objective. Recording times were in the range 1-10 minutes, depending on light intensity, spectral line and photographic emulsion.

Figure B.2 shows the spectroheliograph today. The old photographic arms (A1 for Hα and CaII K) and A2 (for CaII K before 1989) are historical and no longer used. The moving plate was replaced in 2002 by a fixed back illuminated CCD (20 μm square pixels, 14 bits, bandpass identical to the photographic version, 1.5 arcsec/pixel) located inside the spectrograph, with a new optical magnification of 0.7. Figure B.2 displays also the old visual spectrohelioscope (Hale, 1929a) composed of a high speed rotating prism which was inserted in the image plane and an ocular (S) to observe the output slit in the spectrum (A1). In order to make long exposure observations of prominences without disk saturation, an artificial moon of neutral density 1 (ND1) attenuates the brightness of the solar surface; it is driven by a mechanical coupling (N) with the entrance objective motion. Figure B.3 presents typical images obtained daily since 1908 (250 to 300 days/year according to the meteorological conditions).

The photographic plate collection (86 mm images) is under digitization. The first pass is achieved. It is a low resolution scan (2.4 arcsec/pixel, 250 dpi, 8 bits JPEG) which concerns all images (from 1908 to 2001), except the 1914-1918 period corresponding to the first world war (no observers). However, some 16 bits TIFF scans, at the same resolution, have been performed from 1929 to 1937 and 1968 to 1971. Images available between 1893 and 1907, before systematic observations, have also been processed. A second digitization of the entire collection is in course, with much better resolution (1.0 arcsec/pixel, 600 dpi) in 16 bits TIFF format, also converted to FITS. The pixel size is well suited for the current seeing of 2 arcsec. Today, intervals 1937-1967, 1982-1984 and 1997-2001 of the second digitization are available on line, and the remaining part will be achieved in two or three years. Data links are given in Appendix A.

3. Synoptic maps and tables of solar activity

D'Azambuja (1929) started in 1919 the synoptic map program, a complex work which extended continuously from rotation 876 (March 1919) to rotation 2008 (October 2003), as shown in Figure B.4. Unfortunately, we had to stop the collection at the retirement of the last drawer. Many improvements were incorporated during this long period and are de-

scribed by D'Azambuja (1947) and, more recently, by Mouradian (1998). Images of the Sun with a photographic grid of heliographic coordinates were transformed into rectangular maps with an anamorphic optical system designed by Servajean in 1949. Filaments, sunspots and facular plages were manually reported, respectively from Hα, CaII K1v and CaII K3 spectroheliograms. When observations were lacking (clouds), those of Coimbra were used instead. Each rotation was accompanied by tables (today converted to TXT or CSV formats) with many informations, such as filament lengths, prominence heights, "disparition brusque" phenomena, coordinates, center of gravity, dates, durations, radial velocity estimates (1-10 index), characteristics and significance numbers (1-10 index) related to the importance of the features. For ARs, this index was evaluated from the lifetime, the intensity and the area covered by sunspots and plages. Synoptic maps and tables for filaments are available on line at Meudon (Appendix A); other tables for plages can be downloaded from NOAA/NCEI (Appendix A). Maps and tables were also monthly published in the journal "L'Astronomie". Figure B.5 displays an example of data extracted from tables available at NOAA/NCEI between 1919 and 1957, such as filament maximum lengths and importance index, or between 1957 and 1989, such as prominence heights and AR significance index.

Solar filaments are the tracers of magnetic inversion lines at the surface of the Sun, and delineate regions of opposite polarities. Synoptic maps of filaments, coupled with polarization measurements in prominences, allowed Leroy et al. (1983) to identify the magnetic field of quiescent structures (direct or inverse polarity) and discriminate between models proposed by Kippenhahn & Schlüter (1957) and Kuperus & Raadu (1974).

Meudon spectroheliograms were also used, together with data from many observatories, for the international catalog of flare observations. The Meudon group was responsible of the flare section of the Quarterly Bulletin on Solar Activity (QBSA). The catalog was initiated by d'Azambuja in 1934 and published until 1989. The spectroheliograph also contributed to the CaII flocculi section (1917-1944), in collaboration with Arcetri, Kodaikanal, Mount Wilson and Tokyo. The QBSA was distributed in 60 countries around the world. There is a digitized archive on line at Mitaka, NAOJ, Japan (link in appendix).

Besides the sophisticated drawing of Meudon synoptic maps, which combined three different sources (Hα, CaII K1v and CaII K3), McIntosh at Boulder had a similar approach (Webb et al., 2017), combining Hα for filaments, HeI 10830 Å and magnetograms for polarities (rotations 1355-2086 from 1964 to 2009). Chatterjee et al. (2016) and Sheeley et al. (2011) directly processed digitized spectroheliograms and produced CaII K Carrington rotation images, respectively from the Kodaikanal (1907-2007) and the Mount Wilson (1915-1985) collections. Chatterjee et al. (2017) computed, in the same way, Carrington maps of Hα filaments from the Kodaikanal data.

Long-term archives are useful to investigate the spatio-temporal behavior of large-scale structures (such as filaments which are above magnetic polarity inversion lines) and their time evolution, together with their relationship to the magnetic cycle and polar field reversal (recorded at Mount Wilson and Wilcox observatories). An association between filaments and polar field build-up was suggested by Mazumder et al. (2018) from analysis of the McIntosh database. Mazumder et al. (2021) studied filament evolutions over one century using both the Meudon and McIntosh data-sets. Constraining the polar field variation is an important challenge, because it acts as a precursor of the strength of the upcoming sunspot cycle (Bhowmik & Nandy, 2018). Meudon observations of the rush of quiescent filaments towards the poles can serve as tracers of the polar field. Nandy (2021) showed that methods using polar field constraints seem to perform better to predict the sunspot activity cycle.

4. Rare events and rare observations

The long collection of Meudon spectroheliograms is a precious tool to recover past solar activity, variability, and study rare events. Figure B.6 situates in time some examples of uncommon phenomena. We have reported in this figure data of the sunspot area catalog since 1874, revisited by Mandal et al. (2020) and available at the "Centre de données Stellaires" (CDS) at Strasbourg, with a threshold of 0.125% of the hemisphere. Plage areas above 3%, issued from the composite series 1892-2019 of Chatzistergos et al. (2020), also on line at the CDS, are indicated. High energy X-class flares (1-28 intensity range) of GOES/NASA satellites are superimposed. Letters identify rare events and refer to Figures B.7, B.8 and B.9.

4.1. Rare events

S1, S2 and S3 of Figure B.6 are huge sunspot groups, covering up to 5% of the hemisphere, which occurred during cycle 18; some of them (1946, 1947, 1951) are displayed in Figure B.7 in CaII K1v. The size of sunspots is an essential proxy of the magnetic energy that can be dissipated in flares. Aulanier et al. (2013) considered the maximum size of historical sunspots and found that the energy of solar flares cannot exceed 5 10^{26} J (10 times the X17.2 "Halloween" flare of 28 October 2003).

F1, F2, F3 and F4 of Figure B.6 are related to extremely long quiescent filaments (more than one solar radius) in Hα. They delineate large cells of opposite magnetic polarities. Schmieder et al. (1984) observed systematic upward motions in such quiescent filaments, and suggested a relationship with photospheric motions of hypothetic giant convective cells. Their existence was confirmed a few years ago by Hathaway et al. (2014) from SDO/HMI Doppler-shift observations.

P1 and P2 of Figure B.6 indicate historical eruptive prominences (1919, 1925), respectively shown in Figures B.9 and B.12. At that epoch, high cadence filters and coronagraphs did not exist, so that low cadence observations of CaII K spectroheliographs were undertaken. An artificial moon occulted the disk to perform long exposures; it was replaced later by a transparent (ND1) attenuator to observe properly both prominences and the disk.

At last, E1 and E2 of Figure B.6 refer to major solar flares. E2 is the famous X17.2 flare of 18 October 2003 (context shown

by Figure B.3). E1 is the large historical flare of Figure B.9 (25 July 1946, D'Azambuja et al. (1946)) with a series of Hα spectroheliograms, together with the HeI D3 line (previously discovered by Janssen and Lockyer in 1868). Motion picture observations were not common before the 1957 IGY, when filters were progressively introduced. The potential of HeI D3 spectroheliograms was analysed later by Chapman (1972) and D3 line profiles were discussed by Labonte (1977).

4.2. Observations of the Hydrogen Balmer series

Figure B.10 shows exceptional observations made by D'Azambuja in August 1947 showing the different aspects of the Sun in Hα, Hβ, Hγ, Hδ and Hϵ (in the red wing of CaII H), together with the usual CaII K3 spectroheliogram. These observations revealed decreasing contrasts of plages and filaments in blue and violet Balmer lines, as mentioned and discussed by D'Azambuja (1938). For that reason, they were never done on a regular basis.

4.3. CaII K as a proxy for past magnetism and irradiance reconstruction

Ermolli et al. (2018) emphasized the potential of CaII K observations for recovering past solar activity, variability, magnetism and irradiance. Long series of CaII K observations exist in various places, such as Coimbra (1926-now), Kodaikanal (1907-1999), Mitaka (1917-1974), Mount Wilson (1915-1985) and Meudon (1893-now, the longest collection). Chatzistergos et al. (2016) and Chatzistergos et al. (2020) described new methods to combine and cross-calibrate various data-sets and built a plage area composite series (1892-2019), available on line at the CDS. Pevtsov et al. (2016) succeeded to reconstruct pseudo-magnetograms from CaII K observations and sunspot field measurements (for polarities), while Chatzistergos et al. (2019) showed how to recover the unsigned photospheric magnetic field only from CaII K observations, from comparisons of PSPT/Roma images and SDO/HMI magnetic data. The goal is the reconstruction of the past total solar irradiance (TSI) via the SATIRE model, after conversion of CaII K long archives to unsigned magnetic maps. The Spectral And Total Irradiance REconstruction semi empirical model (Yeo (2014) and Yeo et al. (2014)) is based on the coverage of brightness structures and magnetograms. The preliminary results (Chatzistergos et al., 2021) demonstrate that the reconstruction is in good agreement with the TSI composite series of space observations compiled at the Physikalisch Meteorologische Observatorium Davos (PMOD-World Radiation Center) since 1982.

4.4. Line of sight (LOS) velocities

Between April 1909 and November 1943, a high dispersion spectroheliograph dedicated to systematic measurements of LOS velocities (called in french "enregistreur des vitesses radiales") was running in CaII K together with the two spectroheliographs producing monochromatic images in Hα and CaII K (called "enregistreurs des formes"). All instruments shared the same entrance objective and slit. But contrarily to the standard procedure (continuous scans and thin output slit in the spectrum), the entrance objective was not moving at constant speed, but by steps of 22 arcsec (89 steps covering the solar disk forming 89 spectral sections), so that observations were obtained successively. The output slit was enlarged in order to register the full line profiles (2.15 Å spectral range), from which qualitative Doppler-shifts were estimated (and reported in tables). The recording time was in the range 5-15 minutes for the 89 cross sections of the Sun. Figure B.11 shows CaII K observations of 17 September 1938 with the spectrographs, delivering K3 intensities (continuous scan, left) and spectra for 89 cross sections of the Sun (middle). At right is the first worldwide spectroheliogram in HeI 10830 Å reported by D'Azambuja (1938), for the same day; this is a rare observation never systematically reproduced. Daily observations of HeI 10830 Å started much later (1974) at Kitt Peak Vacuum Telescope (Harvey & Sheeley (1977), see also the review of infrared solar physics by Penn (2014)). Figure B.12 shows the eruptive prominence of 18 June 1925, with the CaII K emission spectra by 22 arc sec steps (left, the disk is saturated) and a series of classical CaII K3 images (right). Numerous major events can be found in the historical collection.

5. The new capabilities of the 2018 version

The 2018 version of Meudon spectroheliograph is greatly improved and inspired of the previous system dedicated to the LOS velocity measurements from line profiles ("enregistreur des vitesses"). Technical details can be found in Malherbe & Dalmasse (2019). We just emphasize here the new capabilities. The detector is a high speed sCMOS sensor (100 frames/s, 16 bits, 6.5 μm pixel). The magnification of the spectrograph is 0.31. During the translation of the entrance objective at constant speed, the fast detector registers full line profiles of Hα, CaII H and CaII K (both lines are observed simultaneously). The spectral windows are displayed in Figure B.13 (40 pixels of 0.155 Å for Hα and 2×100 pixels of 0.093 Å for CaII H and K). The maximum spectral resolution is, for Hα and CaII lines, respectively 0.25 Å and 0.15 Å; each data-cube is software calibrated by comparison to atlas profiles (Delbouille et al., 1973) and the result is written in FITS keywords. Larger windows can be chosen upon request (this will not affect the scanning time, only the file size). The recording time of 2048 x-positions of the slit (delivering 2048 [y, λ] slices) varies according to the line, the height of the Sun and sky conditions. Hα data are acquired in 20-30 s, while CaII data need 30-40 s. With the neutral density (ND1), used to observe both the solar disk and prominences, the integration time lies in the range 60-120 s. Hence, this powerful design produces (x, y, λ) data-cubes, which are corrected of the line inclination and curvature, and rotated to present the solar north up. Classical images are (x, y) slices of the data-cubes at fixed wavelength. The spatial pixel size is 1.08 arcsec. In Appendix B, movie 1 shows spectra and scans of 28 October 2021, while movie 2 explores the resulting data-cubes of the three lines, both for standard observations and for long exposure observations of prominences with the ND1 disk attenuator.

Figure B.14 shows the line profile sampling of the three successive versions: photographic until 2001 (monochromatic), CCD from 2002 to 2017 (5 spectral pixels) and sCMOS since 2018 (up to 100 spectral pixels, more upon request). Observations generate data-cubes (x, y, λ) of the full Sun, so that this new capability is probably unique worldwide in the case of Hα, CaII H and K. This new feature is fully compatible with the past, as images are slices of the cubes, and complementary to fast cadence monochromatic or tunable filters. Linsky & Avrett (1970) showed the interest of simultaneous observations of CaII H and K, formed at different altitudes, and Bjørgen et al. (2018) proposed 3D numerical models of both lines in the solar atmosphere. Figure B.15 shows examples of Hα, CaII H and K line profiles obtained in AR2887 and AR2889, for three locations (plages A and C, sunspot B) on 28 October 2021, a couple of hours before the first X-class flare of cycle 25 (X1.0), which occurred in AR2287 at 15:35 UT. Martinez Pillet et al. (1990) investigated the circular polarization of CaII H and K in a sunspot, plage and flare, and showed the possibility to derive the LOS magnetic field at chromospheric levels from Stokes V profiles. Such measurements could be undertaken with Meudon spectroheliograph using a quarter wave plate, a grid and a birefringent polarizing beam splitter-shifter in the image plane with the method developed by Semel (1980).

6. Conclusions

Observations with Deslandres's spectroheliograph started in 1893 at Paris observatory and became systematic in 1908 at Meudon under the auspices of D'Azambuja. It produced monochromatic images and, since 2018, delivers (x, y, λ) data-cubes of full line profiles of Hα, CaII H and K for each point of the solar surface. This unique capability compensates the low cadence of the instrument (a few observations daily). Spectra are not affected by the atmospheric turbulence, because all wavelengths along line profiles are simultaneous, contrarily to tunable filters. The CaII K collection started in 1893 and is probably the longest available, allowing long terms investigations on solar variability, activity, and the reconstruction of past magnetism and irradiance. The instrument is fully complementary to ground-based filter networks, such as the Hα GONG or GHN, or to EUV instruments onboard satellites, such as SOHO/EIT or SDO/AIA, which observe the hotter corona. A second digitization of the photographic collection is in course, with much better resolution and quality than the first one. However, the future after 2027 remains uncertain, due to retirements of observers at the same time, so that a possible collaboration with amateurs is considered. We encourage the solar community to use our data for publications; in that case, please just insert the following acknowledgment: "Meudon spectroheliograph data are courtesy of the solar operational services of Paris Observatory".

7. Disclosure of potential conflicts of interest

The authors declare that they have no conflicts of interest.

8. Acknowledgments

This paper is dedicated to the memory of Lucien d'Azambuja (1884-1970) who organized in 1908 systematic observations of the Sun at Meudon.

The authors thank the two referees and the editor for helpful comments and suggestions. We are indebted to the numerous observers (since 1908 !) and to the technical staff who maintained the spectroheliograph permanently up to date. We acknowledge the observing team for the long work of digitization of the photographic collection. We finally acknowledge the LESIA department, the Scientific Council of Paris Observatory and the INSU/CNRS for financial support.

References

Aulanier, G., Démoulin, P., Schrijver, C. J., Janvier, M., Pariat, E., & Schmieder, B. (2013). The standard flare model in three dimensions. II. Upper limit on solar flare energy. *Astron. Astrophys.*, *549*, A66 (7p). doi:10.1051/0004-6361/201220406. arXiv:1212.2086.

Bhowmik, P., & Nandy, D. (2018). Prediction of the strength and timing of sunspot cycle 25 reveal decadal-scale space environmental conditions. *Nature Communications*, *9*, 5209 (10p). doi:10.1038/s41467-018-07690-0. arXiv:1909.04537.

Bjørgen, J. P., Sukhorukov, A. V., Leenaarts, J., Carlsson, M., de la Cruz Rodríguez, J., Scharmer, G. B., & Hansteen, V. H. (2018). Three-dimensional modeling of the Ca II H and K lines in the solar atmosphere. *Astron. Astrophys.*, *611*, A62 (19p). doi:10.1051/0004-6361/201731926. arXiv:1712.01045.

Chapman, G. A. (1972). Magnetic Fields and Helium-D_3 Spectroheliograms. *Solar Phys.*, *24*(2), 288–300. doi:10.1007/BF00153369.

Chatterjee, S., Banerjee, D., & Ravindra, B. (2016). A Butterfly Diagram and Carrington Maps for Century long Ca II K Spectroheliograms from The Kodaikanal Observatory. *Astrophys. J.*, *827*(1), 87 (11p). doi:10.3847/0004-637X/827/1/87. arXiv:1605.08219.

Chatterjee, S., Hegde, M., Banerjee, D., & Ravindra, B. (2017). Long-term Study of the Solar Filaments from the Synoptic Maps as Derived from Halpha Spectroheliograms of the Kodaikanal Observatory. *Astrophys. J.*, *849*(1), 44 (8p). doi:10.3847/1538-4357/aa8ad9. arXiv:1707.05658.

Chatzistergos, T., Ermolli, I., Krivova, N. A., Solanki, S. K., Banerjee, D., Barata, T., Belik, M., Gafeira, R., Garcia, A., Hanaoka, Y., Hegde, M., Klimeš, J., Korokhin, V. V., Lourenço, A., Malherbe, J.-M., Marchenko, G. P., Peixinho, N., Sakurai, T., & Tlatov, A. G. (2020). Analysis of full-disc Ca II K spectroheliograms. III. Plage area composite series covering 1892-2019. *Astron. Astrophys.*, *639*, A88 (22p). doi:10.1051/0004-6361/202037746. arXiv:2005.01435.

Chatzistergos, T., Ermolli, I., Solanki, S. K., & Krivova, N. A. (2016). Exploiting Four Historical Ca II K Spectroheliogram Archives. In I. Dorotovic, C. E. Fischer, & M. Temmer (Eds.), *Coimbra Solar Physics Meeting: Ground-based Solar Observations in the Space Instrumentation Era* (pp. 227–230). volume 504 of *Astronomical Society of the Pacific Conference Series*.

Chatzistergos, T., Ermolli, I., Solanki, S. K., Krivova, N. A., Giorgi, F., & Yeo, K. L. (2019). Recovering the unsigned photospheric magnetic field from Ca II K observations. *Astron. Astrophys.*, *626*, A114 (17p). doi:10.1051/0004-6361/201935131. arXiv:1905.03453.

Chatzistergos, T., Krivova, N. A., Ermolli, I., Yeo, K. L., Mandal, S., Solanki, S. K., Kopp, G., & Malherbe, J.-M. (2021). Reconstructing solar irradiance from historical Ca II K observations. I. Method and its validation. *Astron. Astrophys.*, *656*, A104 (23p). doi:10.1051/0004-6361/202141516. arXiv:2109.05844.

Chen, P. F. (2011). Coronal Mass Ejections: Models and Their Observational Basis. *Living Reviews in Solar Physics*, *8*(1), 1 (92p). doi:10.12942/lrsp-2011-1.

D'Azambuja, L. (1920a). Le Spectroheliographe et les Photographies Quotidiennes de l'Atmosphere du Soleil (the spectroheliograph and daily photographs of the solar atmosphere). *L'Astronomie*, *34*, 433–446.

D'Azambuja, L. (1920b). Le Spectroheliographe (the spectroheliograph). *L'Astronomie*, *34*, 487–498.

D'Azambuja, L. (1929). L'Activite Solaire (solar activity). *L'Astronomie*, *43*, 135–138.

D'Azambuja, L. (1938). Images Nouvelles de la Chromosphere Solaire Obtenues au Spectroheliographe avec la Raie Infrarouge de l'Helium 10830 et avec la Raie Hepsilon de l'Hydrogene (new spectroheliograms of the solar chromosphere in the IR Helium 10830 line and Hepsilon Hydrogen line). *Bulletin Astronomique*, *11*, 349–359.

D'Azambuja, M. (1947). L'Activité Solaire, Cartes synoptiques de la chromosphère et des taches (solar activity, synoptics charts of the chromosphere and sunspots). *L'Astronomie*, *61*, 25–28.

D'Azambuja, M., Servajean, R., Olivieri, G., & Guimont, J. E. (1946). L'Activité Solaire (solar activity). *L'Astronomie*, *60*, 213–219.

Deherain, H. (1929). *Oeuvres scientifiques recueillies et publiees par Henri Deherain (scientific works of Jules Janssen gathered and published by Henri Deherain)*. Societe des Editions Maritimes, geographiques et Coloniales, Paris.

Delbouille, L., Roland, G., & Neven, L. (1973). *Atlas photometrique du spectre solaire de [lambda] 3000 a [lambda] 10000 (photometric atlas of the solar spectrum from 3000 to 10000 Angstrom)*. Université de Liège.

Deslandres, H. (1908). Reports of Committees and Papers communicated to the Solar Union. No. 11. Enregistrement de la surface et de l'atmosphère solaire à l'Observatoire de Meudon (recording the solar surface and atmosphere at Meudon Observatory). *Transactions of the International Union for Cooperation in Solar Research*, *2*, 232–244.

Ermolli, I., Chatzistergos, T., Krivova, N. A., & Solanki, S. K. (2018). The potential of Ca II K observations for solar activity and variability studies. *IAU Symposium*, *340*, 115–120. doi:10.1017/S1743921318001849. arXiv:1805.04483.

Ermolli, I., Marchei, E., Centrone, M., Criscuoli, S., Giorgi, F., & Perna, C. (2009). The digitized archive of the Arcetri spectroheliograms. Preliminary results from the analysis of Ca II K images. *Astron. Astrophys.*, *499*(2), 627–632. doi:10.1051/0004-6361/200811406.

Hale, G. E. (1907). Some new applications of the spectroheliograph. *Contributions from the Mount Wilson Observatory / Carnegie Institution of Washington*, *18*, 1–3.

Hale, G. E. (1929a). The Spectrohelioscope and its Work. *Astrophys. J.*, *70*, 265–311. doi:10.1086/143226.

Hale, G. E. (1929b). The spectroscope and its work. Part I. History, instruments, adjustments, and methods of observation. *Contributions from the Mount Wilson Observatory / Carnegie Institution of Washington*, *388*, 1–47.

Hanaoka, Y. (2013). Long-term synoptic observations of the Sun at the National Astronomical Observatory of Japan. In *Journal of Physics Conference Series* (p. 012041 (4p)). volume 440 of *Journal of Physics Conference Series*. doi:10.1088/1742-6596/440/1/012041.

Harvey, J. W., Bolding, J., Clark, R., Hauth, D., Hill, F., Kroll, R., Luis, G., Mills, N., Purdy, T., Henney, C., Holland, D., & Winter, J. (2011). Full-disk Solar H-alpha Images From GONG. In *AAS/Solar Physics Division Abstracts #42* (p. 17.45). volume 42 of *AAS/Solar Physics Division Meeting*.

Harvey, J. W., & Sheeley, J., N. R. (1977). A comparison of HeII 304 Å and HeI 10830 Å spectroheliograms. *Solar Phys.*, *54*(2), 343–351. doi:10.1007/BF00159924.

Hathaway, D. H. (2010). The Solar Cycle. *Living Reviews in Solar Physics*, *7*(1), 1 (65p). doi:10.12942/lrsp-2010-1.

Hathaway, D. H., Upton, L., & Colegrove, O. (2014). Giant Convection Cells Found on the Sun. *arXiv e-prints*, (p. arXiv:1401.0551). arXiv:1401.0551.

Kippenhahn, R., & Schlüter, A. (1957). Eine Theorie der solaren Filamente. Mit 7 Textabbildungen (a theory of solar filaments). *Zeitschrift fur Astrophysik*, *43*, 36–62.

Kuperus, M., & Raadu, M. A. (1974). The Support of Prominences Formed in Neutral Sheets. *Astron. Astrophys.*, *31*, 189–193.

Labonte, B. J. (1977). A measurement of the helium D_3 profile with a birefringent filter. *Solar Phys.*, *53*(2), 369–374. doi:10.1007/BF00160280.

Lefebvre, S., Ulrich, R. K., Webster, L. S., Varadi, F., Javaraiah, J., Bertello, L., Werden, L., Boyden, J. E., & Gilman, P. (2005). The solar photograph archive of the Mount Wilson Observatory. A resource for a century of digital data. *Mem. Societa Astronomica Italiana.*, *76*, 862–867.

Leroy, J. L., Bommier, V., & Sahal-Brechot, S. (1983). The Magnetic Field in the Prominences of the Polar Crown. *Solar Phys.*, *83*(1), 135–142. doi:10.1007/BF00148248.

Linsky, J. L., & Avrett, E. H. (1970). The Solar H and K Lines. *Pub. Astron. Soc. Pac.*, *82*(485), 169–248. doi:10.1086/128904.

Lourenço, A., Carvalho, S., Barata, T., Garcia, A., Carrasco, V., & Peixinho, N. (2019). Solar observations at the Coimbra Astronomical Observatory. *Open Astronomy*, *28*(1), 165–179. doi:10.1515/astro-2019-0015.

Lyot, B. (1944). Le Filtre Monochromatique Polarisant et ses Applications en Physique Solaire (The monochromatic polarizing filter and its applications to solar physics). *Annales d'Astrophysique*, *7*, 31–79.

Malherbe, J. M., & Dalmasse, K. (2019). The New 2018 Version of the Meudon Spectroheliograph. *Solar Phys.*, *294*(5), 52 (14p). doi:10.1007/s11207-019-1441-7.

Mandal, S., Krivova, N. A., Solanki, S. K., Sinha, N., & Banerjee, D. (2020). Sunspot area catalog revisited: Daily cross-calibrated areas since 1874. *Astron. Astrophys.*, *640*, A78 (12p). doi:10.1051/0004-6361/202037547. arXiv:2004.14618.

Martinez Pillet, V., Garcia Lopez, R. J., del Toro Iniesta, J. C., Rebolo, R., Vazquez, M., Beckman, J. E., & Char, S. (1990). Circular Polarization of the CA II H and K Lines in Solar Quiet and Active Regions. *Astrophys. J. Lett.*, *361*, L81–L85. doi:10.1086/185832.

Mazumder, R., Bhowmik, P., & Nandy, D. (2018). The Association of Filaments, Polarity Inversion Lines, and Coronal Hole Properties with the Sunspot Cycle: An Analysis of the McIntosh Database. *Astrophys. J.*, *868*(1), 52 (10p). doi:10.3847/1538-4357/aae68a. arXiv:1810.02133.

Mazumder, R., Chatterjee, S., Nandy, D., & Banerjee, D. (2021). Solar Cycle Evolution of Filaments over a Century: Investigations with the Meudon and McIntosh Hand-drawn Archives. *Astrophys. J.*, *919*(2), 125 (13p). doi:10.3847/1538-4357/ac09f6. arXiv:2106.04320.

McMath, F. C., McMath, R. R., & Hulbert, H. S. (1932). Some new methods in astronomical photography, with application to moving pictures of celestial objects. *Publications of Michigan Observatory*, *4*(4), 53–73.

McMath, R. R., & Petrie, R. M. (1934). The spectroheliokinematograph. *Publications of Michigan Observatory*, *5*(8), 103–117.

Mouradian, Z. (1998). The New Solar Activity Synoptic Maps of Observatoire de Paris-Meudon. In K. S. Balasubramaniam, J. Harvey, & D. Rabin (Eds.), *Synoptic Solar Physics* (pp. 197–204). volume 140 of *Astronomical Society of the Pacific Conference Series*.

Nandy, D. (2021). Progress in Solar Cycle Predictions: Sunspot Cycles 24-25 in Perspective. *Solar Phys.*, *296*(3), 54 (29p). doi:10.1007/s11207-021-01797-2. arXiv:2009.01908.

Penn, M. J. (2014). Infrared Solar Physics. *Living Reviews in Solar Physics*, *11*(1), 2 (66p). doi:10.12942/lrsp-2014-2.

Pevtsov, A. A., Virtanen, I., Mursula, K., Tlatov, A., & Bertello, L. (2016). Reconstructing solar magnetic fields from historical observations. I. Renormalized Ca K spectroheliograms and pseudo-magnetograms. *Astron. Astrophys.*, *585*, A40 (9p). doi:10.1051/0004-6361/201526620.

Schmieder, B., Ribes, B., Mein, E., & Malherbe, J. M. (1984). Study of giant cell motions and their possible relationship with the dynamics of filaments. *Mem. Societa Astronomica Italiana.*, *55*(1-2), 319–323.

Schwenn, R. (2006). Space Weather: The Solar Perspective. *Living Reviews in Solar Physics*, *3*(1), 2 (72p). doi:10.12942/lrsp-2006-2.

Semel, M. (1980). A precise optical polarization analyzer. *Astron. Astrophys.*, *91*(3), 369–371.

Sheeley, J., N. R., Cooper, T. J., & Anderson, J. R. L. (2011). Carrington Maps of Ca II K-line Emission for the Years 1915-1985. *Astrophys. J.*, *730*(1), 51 (17p). doi:10.1088/0004-637X/730/1/51.

Steinegger, M., Hanslmeier, A., Otruba, W., Freislich, H., Denker, C., Goode, P. R., Marquette, W. M., Varied, J., Wang, H., Luo, G., Chen, D., & Zhang, Q. (2000). An Overview of the New Global High-Resolution H-alpha Network. *Hvar Observatory Bulletin*, *24*(1), 179–183.

Temmer, M. (2021). Space weather: the solar perspective. *Living Reviews in Solar Physics*, *18*(1), 4 (80p). doi:10.1007/s41116-021-00030-3. arXiv:2104.04261.

Toriumi, S., & Wang, H. (2019). Flare-productive active regions. *Living Reviews in Solar Physics*, *16*(1), 3 (128p). doi:10.1007/s41116-019-0019-7. arXiv:1904.12027.

Webb, D., Gibson, S., Hewins, I., McFadden, R., Emery, B., Denig, W., & McIntosh, P. (2017). Preserving a Unique Archive for Long-Term Solar Variability Studies. *Space Weather*, *15*(11), 1431–1431. URL: https://agupubs.onlinelibrary.wiley.com/doi/abs/10.

1002/swe.20362. doi:10.1002/swe.20362.
Webb, D. F., & Howard, T. A. (2012). Coronal Mass Ejections: Observations. *Living Reviews in Solar Physics*, *9*(1), 3 (83p). doi:10.12942/lrsp-2012-3.
Yeo, K. L. (2014). Analysis and modeling of solar irradiance variations. *arXiv e-prints*, (p. arXiv:1412.3935). arXiv:1412.3935.
Yeo, K. L., Krivova, N. A., Solanki, S. K., & Glassmeier, K. H. (2014). Reconstruction of total and spectral solar irradiance from 1974 to 2013 based on KPVT, SoHO/MDI, and SDO/HMI observations. *Astron. Astrophys.*, *570*, A85 (18p). doi:10.1051/0004-6361/201423628. arXiv:1408.1229.

Appendix A. Useful data links

Meudon and Coimbra spectroheliograms (16 bits FITS, 8 bits JPEG) and Meudon spectral data-cubes (16 bits FITS 3D since 2018):
https://bass2000.obspm.fr/

Meudon collection before 1980:
https://bass2000.obspm.fr/piwigo/index.php?/category/157

Meudon synoptic maps and associated tables:
https://bass2000.obspm.fr/lastsynmap.php
and
https://www.ngdc.noaa.gov/stp/space-weather/solar-data/solar-features/prominences-filaments/filaments/

Quarterly Bulletin on Solar Activity (QBSA):
https://solarwww.mtk.nao.ac.jp/en/wdc/qbsa.html

Mount Wilson CaII K spectroheliograms:
https://www.astro.ucla.edu/~ulrich/MW_SPADP/index.html

Kodaikanal spectroheliograms:
https://kso.iiap.res.in/new/data

Mitaka CaII K spectroheliograms:
https://solarwww.mtk.nao.ac.jp/en/db_ca.html

The Sun and the Earth's climate (Max Planck Iinstitute, Göttingen):
https://www2.mps.mpg.de/projects/sun-climate/data.html

Appendix B. Online material

MPEG4 movie 1: this movie presents the observing procedure of the 2018 version of Meudon spectroheliograph with three line scans, Hα, CaII H and K. CaII H and K are strictly simultaneous. The line profiles are recorded in 3D FITS files, from which classical images are derived as slices. Example of 28 October 2021, the first X-class flare of cycle 25 occurred in the southern AR2287, a couple of hours after the observation. Displayed images are chosen at line centre; for CaII, we took the square-root of intensities to reduce the high dynamics of plages for better visualization.

MPEG4 movie 2: this movie explores the 3D data cubes of 28 October 2021, successively in Hα, CaII H and K for the solar disk (part 1). Long exposure observations for prominences of the same lines (with an artificial ND1 attenuator upon the disk) are also shown in part 2. CaII H and K are always observed simultaneously. The line profile of the disk centre is superimposed with a moving index indicating the wavelength position.

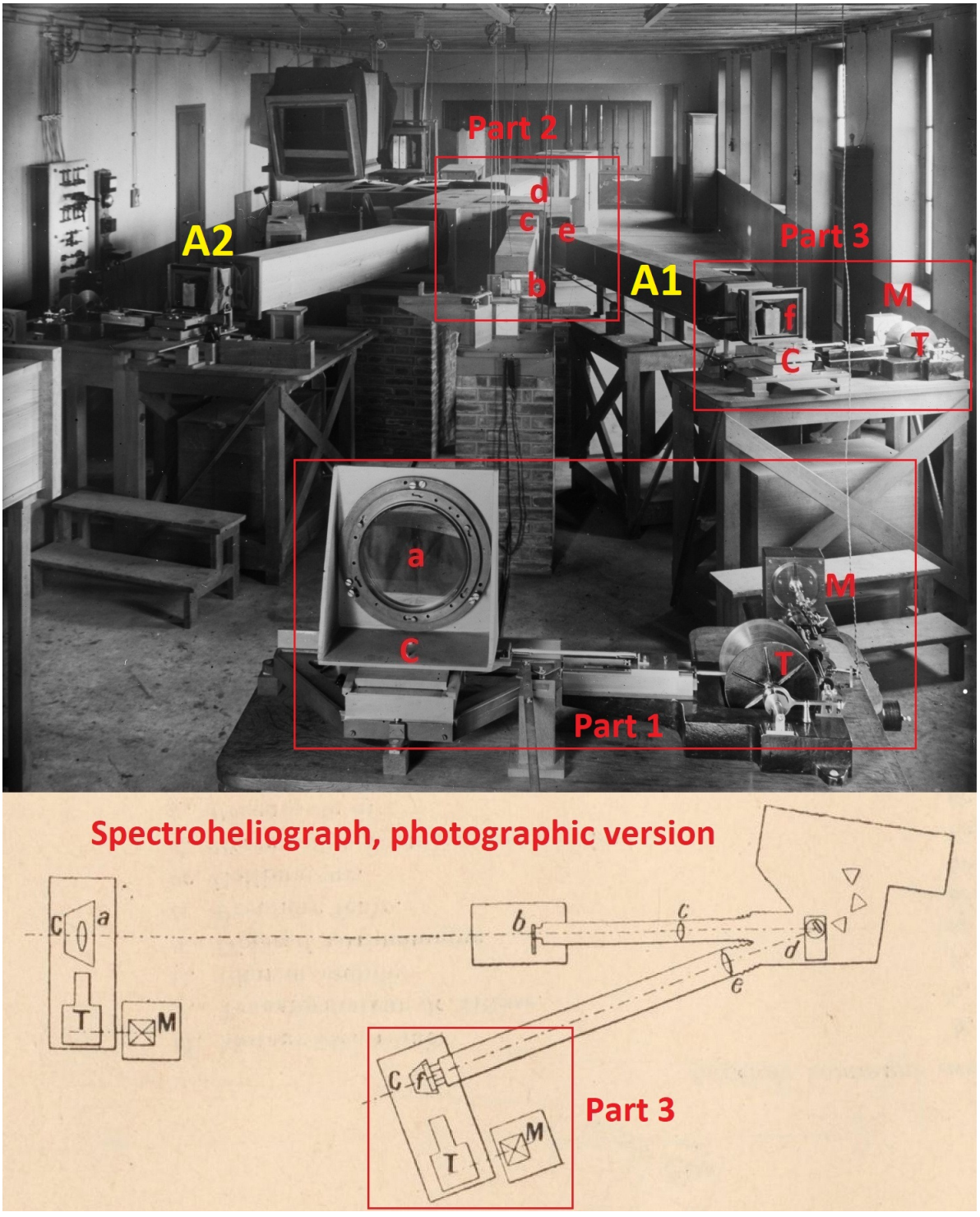

Fig. B.1. Meudon spectroheliograph in 1919. Part 1: entrance with a = imaging objective (250 mm diameter, f = 4000 mm, F/16); C = moving support; T = velocity reductor; M = motor. Part 2: spectrograph with b = entrance slit; c = collimator (f = 1300 mm); d = prisms or grating (300 groves/mm, 17° blaze angle); e = camera lens (f = 3000 mm). Part 3: exit with f = selective slit in the spectrum; C = moving support of photographic plates; T = speed reductor; M = motor. Arms A1 and A2 were used respectively for Hα (Rowland grating) and CaII K (prisms) until 1988. After this date, arm A1 was used for both (new grating). In 2002 and 2018, part 3 was successively replaced by two generations of electronic sensors (CCD, sCMOS) fed by new camera lenses (respectively 900 mm and 400 mm focal length).

Fig. B.2. Meudon spectroheliograph today. b = entrance slit of the spectrograph (30 μm width). A1 and A2 are old photographic arms (chambers not used any more). N is the mechanical coupling between the entrance objective (a) of Figure B.1 and the moving artificial moon (a round neutral density 1 of 37 mm diameter). This attenuator is located in the image plane and avoids the saturation of the disk in the case of prominence observations with long exposure time. S is an old visual flare spectroheliosccope (no more used), composed of a high speed rotating prism which translates active region images upon the slit (b), and an ocular (S) to observe the the wavelength selected by the output slit located in A1.

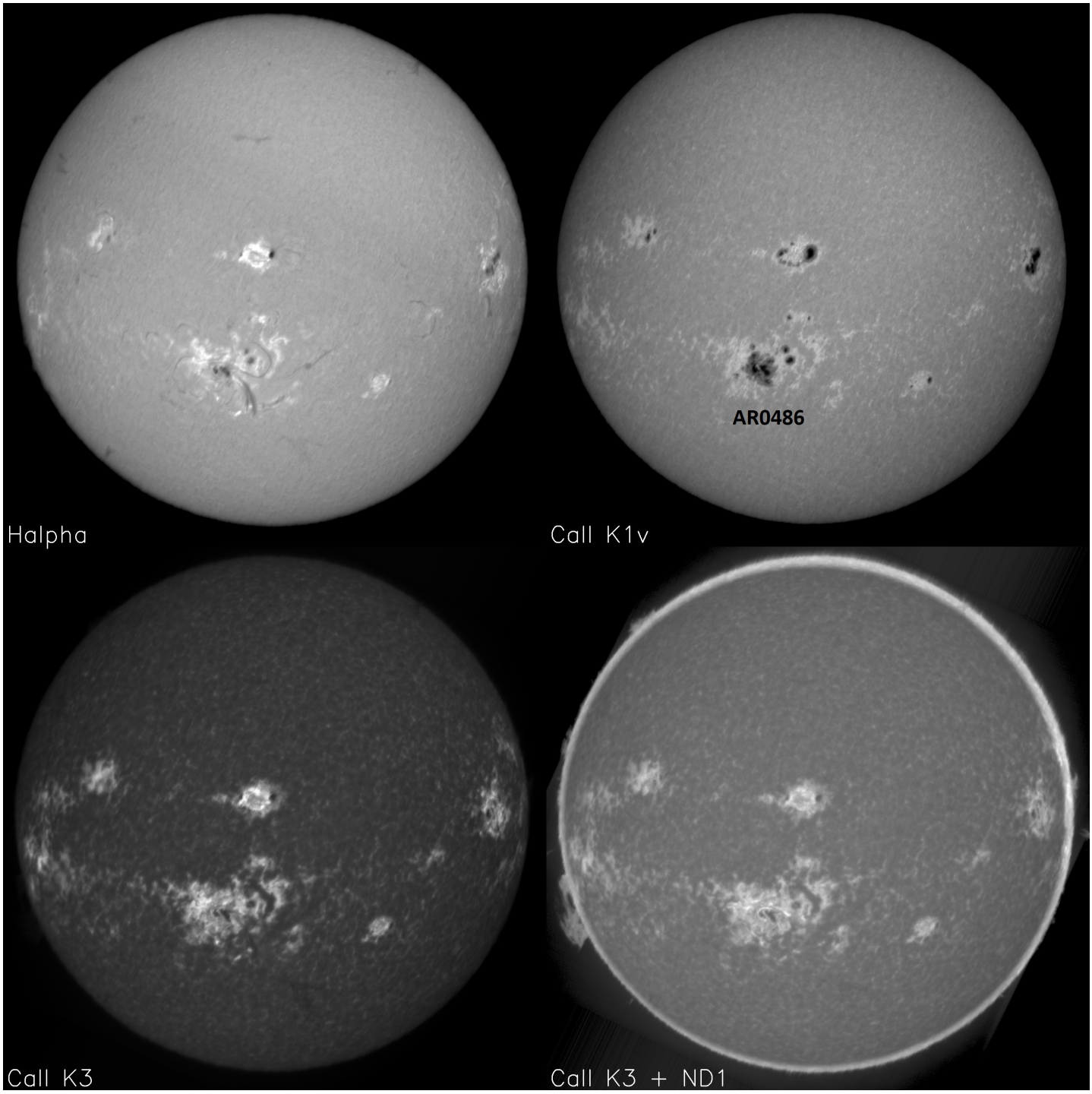

Fig. B.3. Typical images obtained daily at Meudon spectroheliograph. Example of 28 October 2003, a couple of hours before the historic X17.2 flare (11:10 UT) in the big AR0486 of the southern hemisphere. A set of spectroheliograms is composed of Hα centre (08:09 UT), CaII K1v (violet wing at -1.5 Å, 08:13 UT), CaII K3 (line centre, 08:13 UT) and a long exposure CaII K3 with the ND1 artificial moon (08:50 UT) in order to register both prominences and the solar disk.

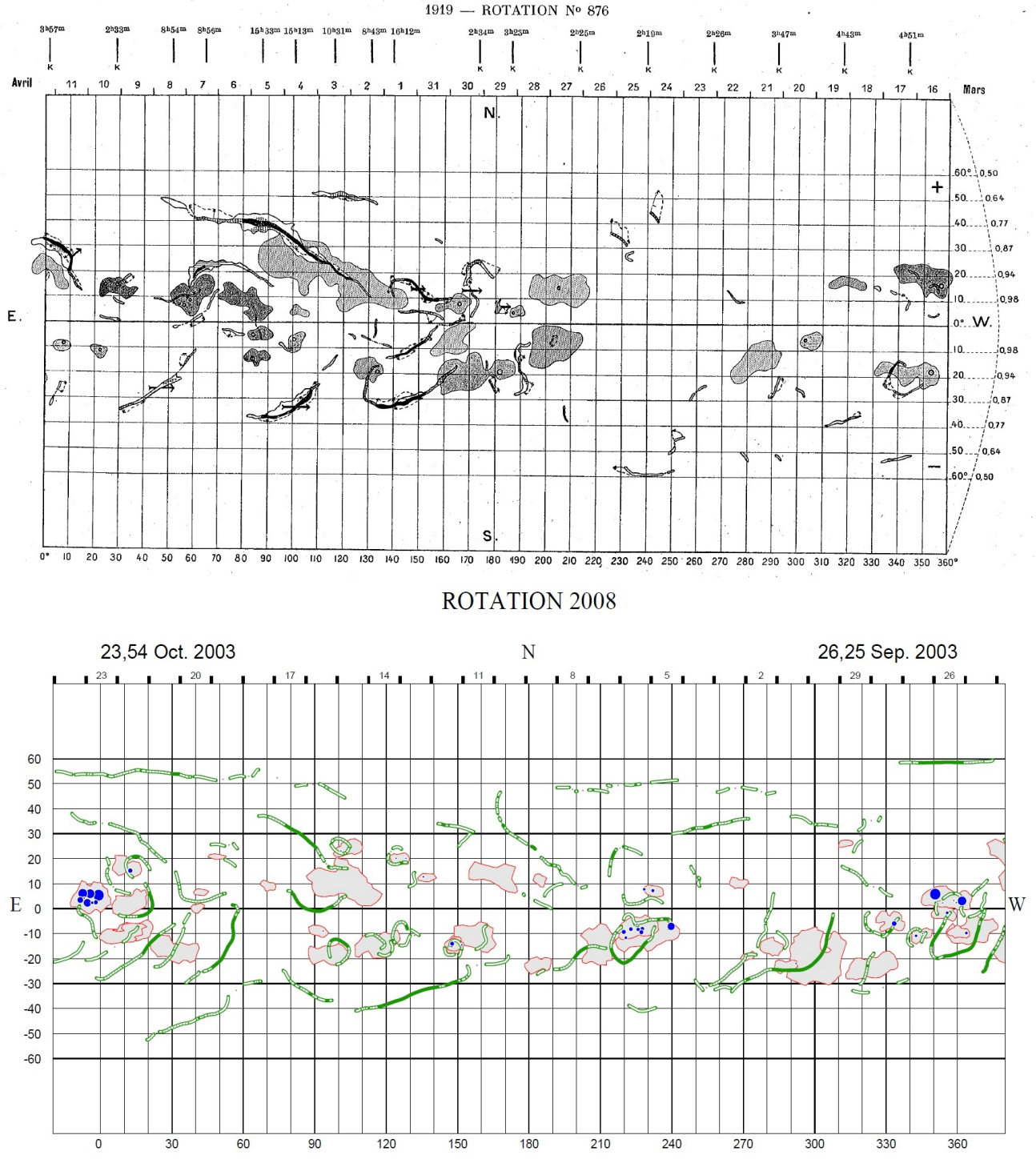

Fig. B.4. Synoptic maps (longitude in abscissa, latitude in ordinates) of filaments, faculae and sunspots. The collection starts at rotation 876 (top) and finishes at rotation 2008 (bottom), and goes from 1919 to 2003. Each map is accompanied by tables providing the main characteristics of observed features (see Figure B.5).

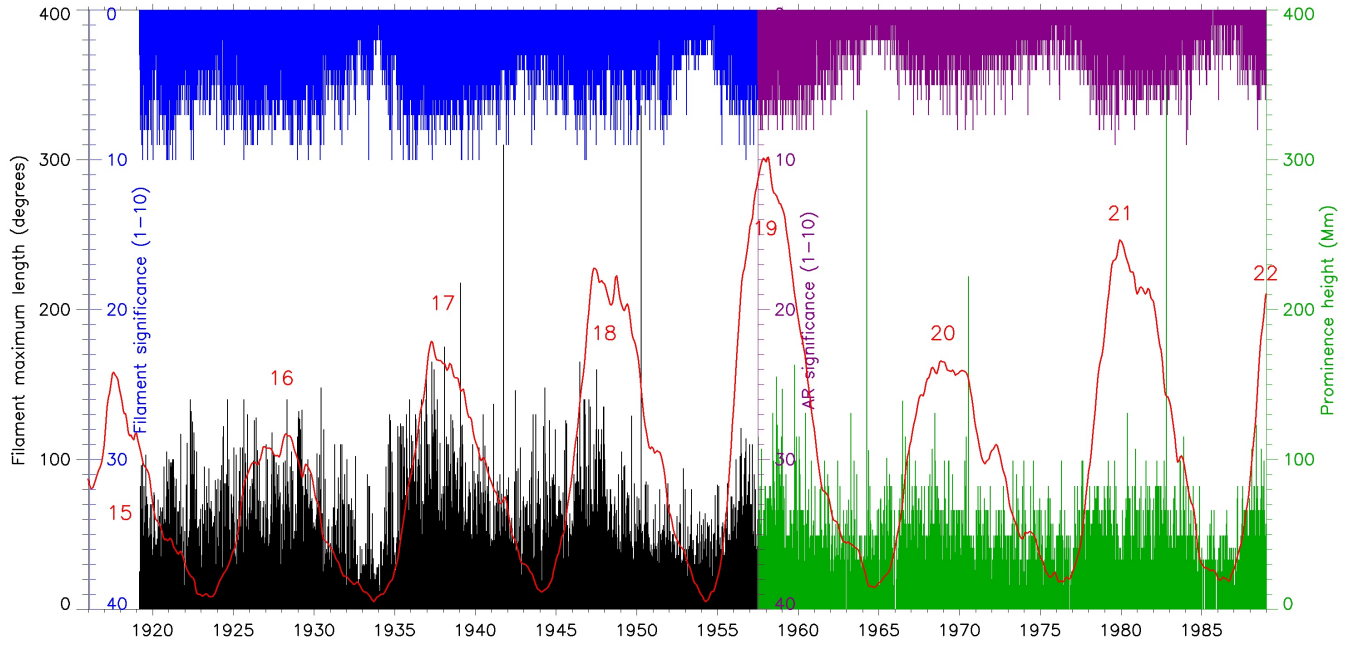

Fig. B.5. Examples of data provided by the tables associated with each Carrington rotation. Black: maximum length of filaments (degrees). Green: maximum height of prominences (Mm). Blue: filament significance (1-10 scale). Violet: active region significance (this index, in the range 1-10, is evaluated from the lifetime, the intensity and the area of facular plages, or the number and the area of sunspots). The Brussels sunspot number has been superimposed in red together with the identification of cycles.

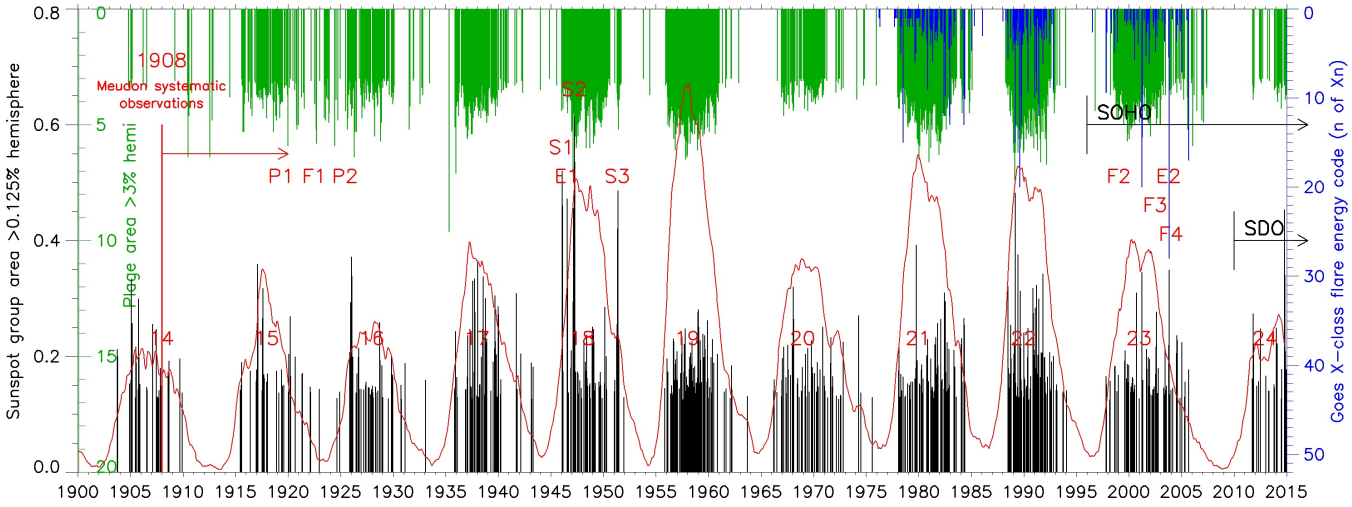

Fig. B.6. Some rare events distribution. Black: sunspot group area above 0.125% of the solar hemisphere (after Mandal et al. (2020)). Green: plage area above 3% of the hemisphere (after Chatzistergos et al. (2020)). Blue: X-class flares (X1 to X28 range). The Brussels sunspot number has been superimposed in red together with identification of cycles. P1, P2 = prominence eruptions of Figures B.9 and B.12. F1, F2, F3, F4 = long filaments of Figure B.8. E1, E2 = strong flares of Figures B.9 and B.3. S1, S2, S3 = huge sunspot groups of Figures B.7. The most significant sunspot groups were seen during cycle 18.

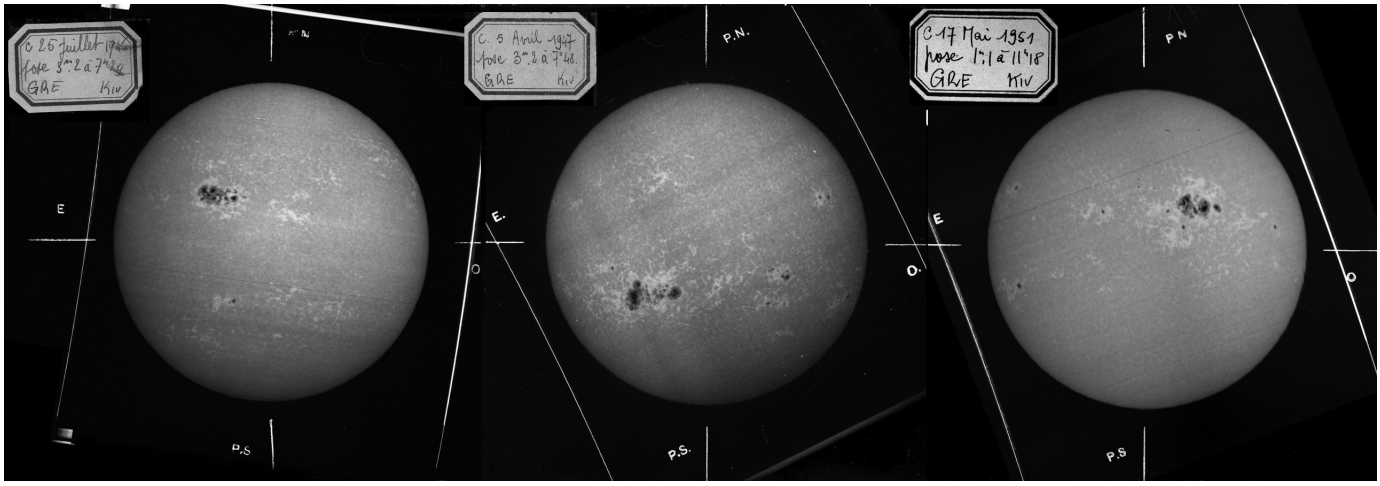

Fig. B.7. Some examples of the huge sunspot groups of cycle 18 (CaII K1v spectroheliograms): from left to right, 25 July 1946, 5 April 1947, 17 May 1951, covering respectively 0.46%, 0.61% and 0.48% of the disk area.

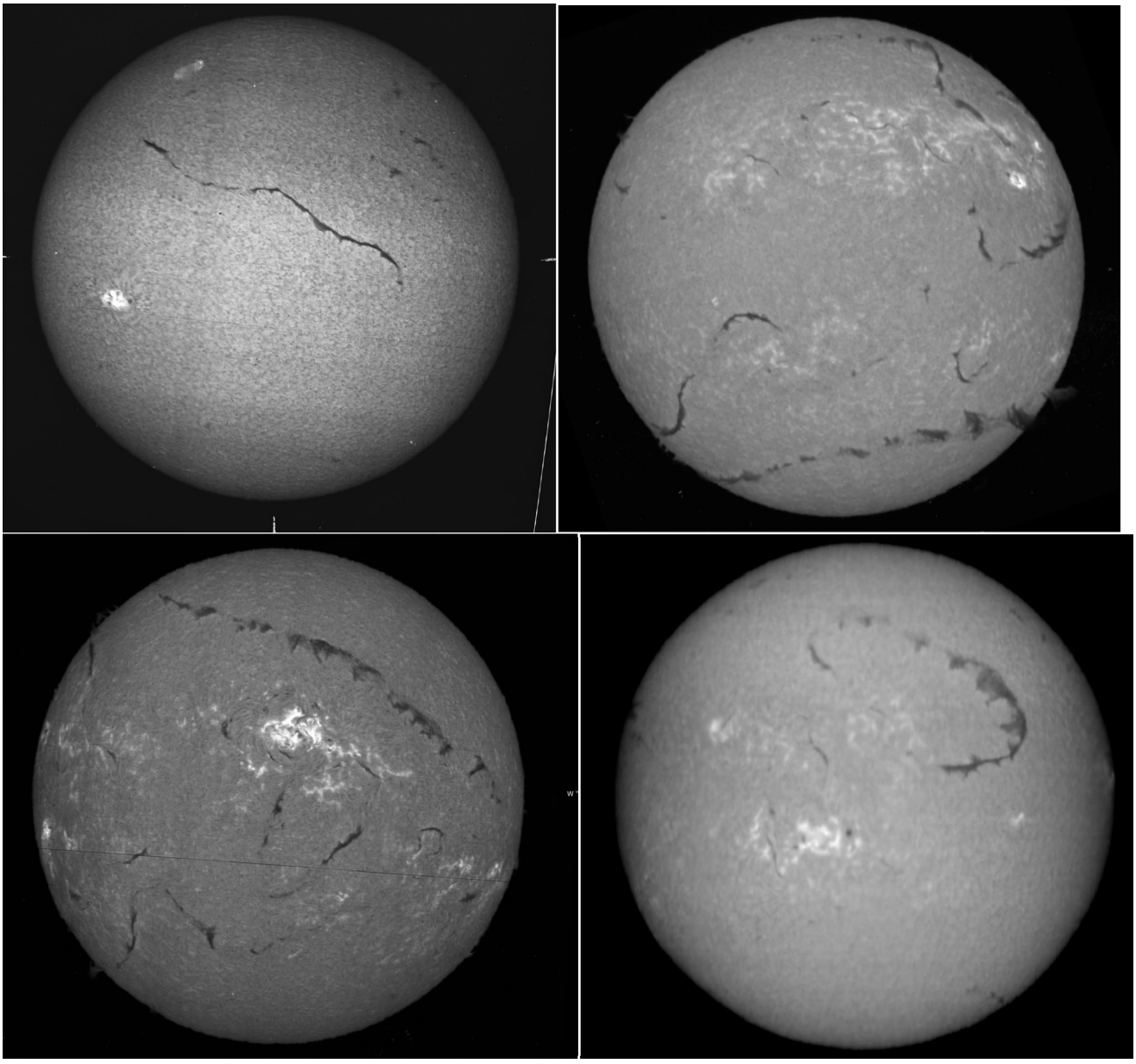

Fig. B.8. Some examples of the longest filaments observed with Meudon spectroheliograph in Hα centre. Top: 20 July 1922 (left) and 30 january 1999 (right). Bottom: 16 July 2002 (left) and 18 January 2004 (right).

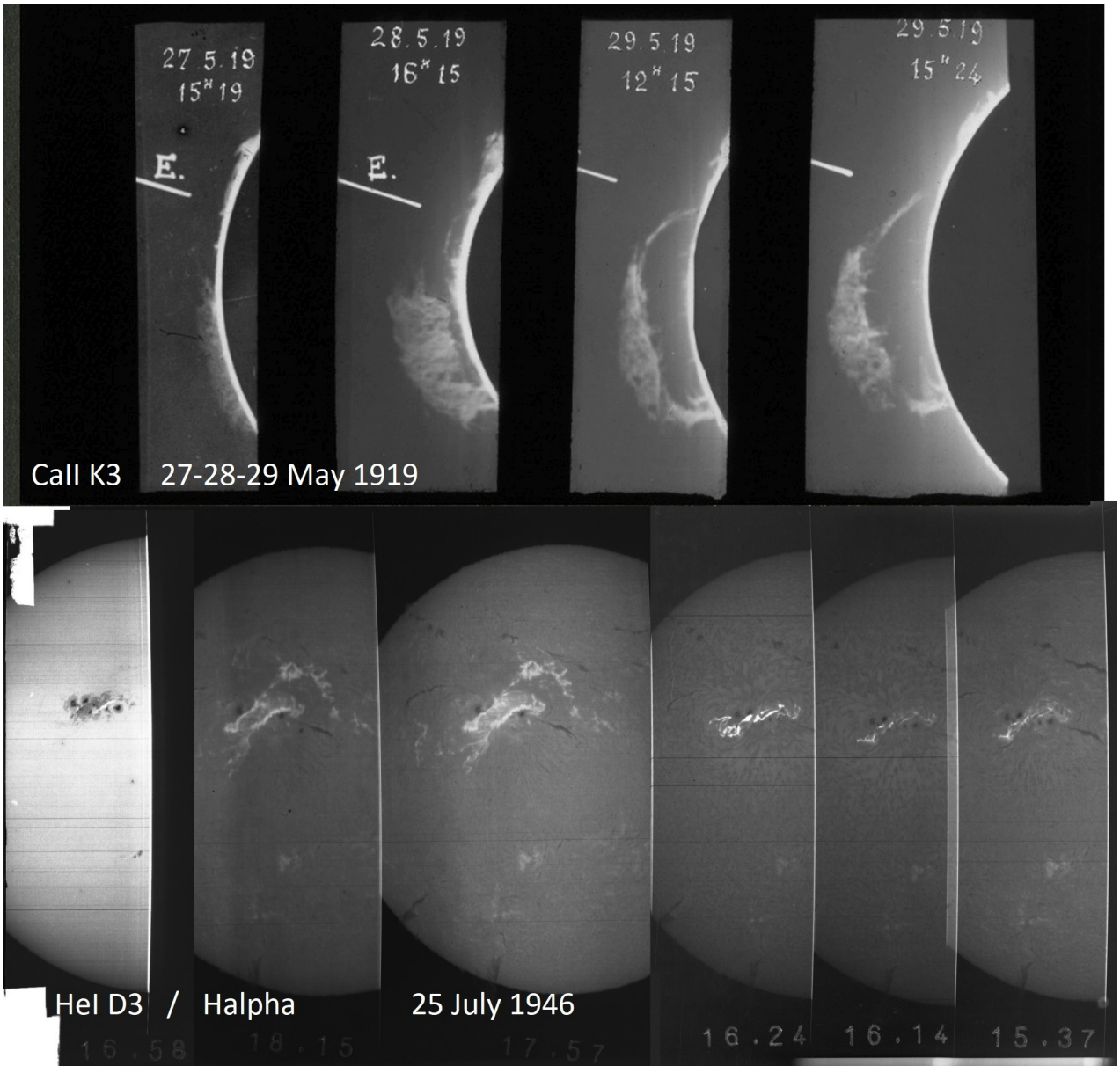

Fig. B.9. Examples of rare dynamic events observed with Meudon spectroheliograph. Top: the eruptive prominence of 27-28-29 May 1919 observed in CaII K3. Bottom: the large solar flare of 25 July 1946 observed in HeI D3 (left panel at 16:58 UT) and in Hα line centre at 18:15, 17:57, 16:24, 16:14 and 15:37 UT (right panels).

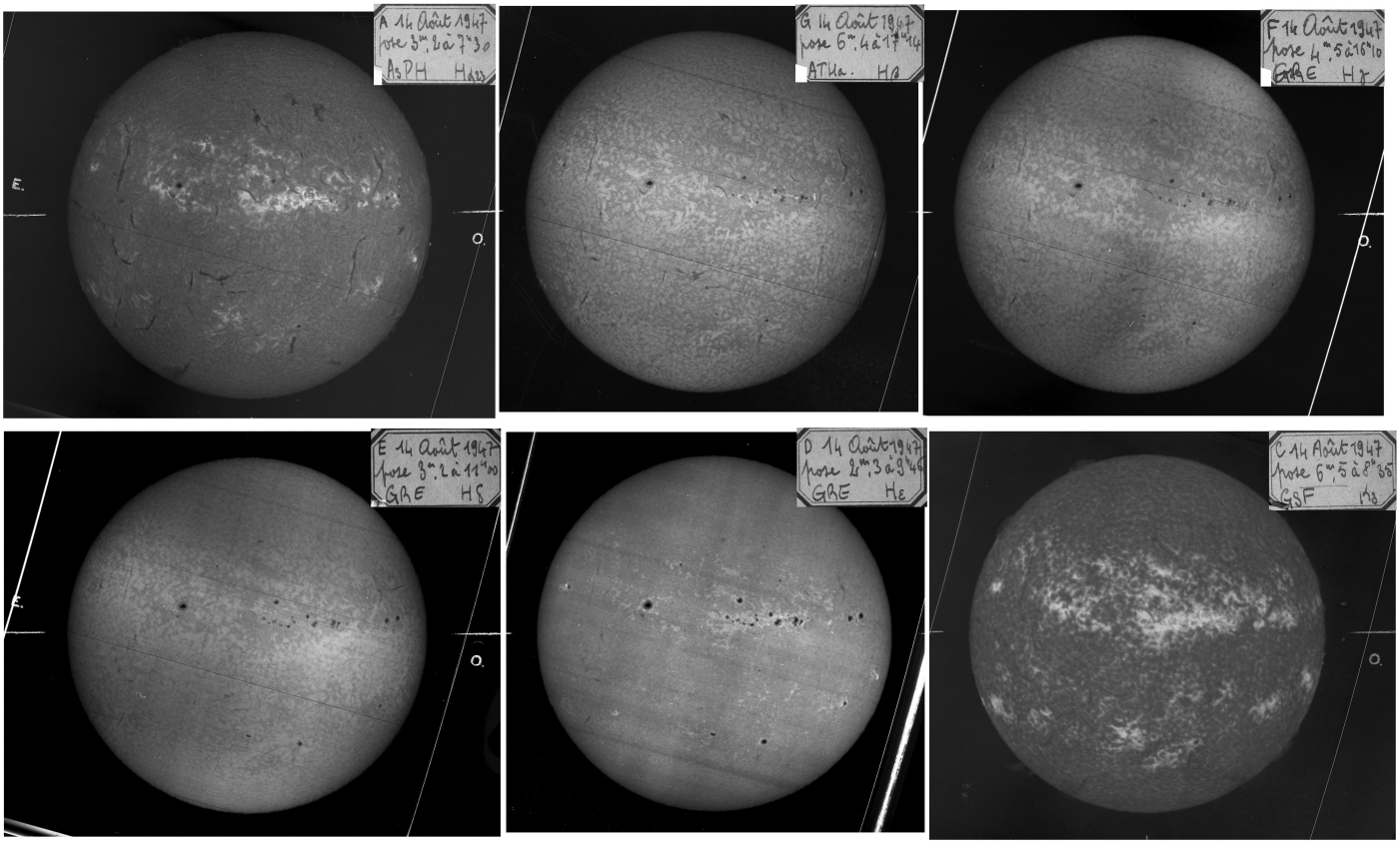

Fig. B.10. Exceptional observations of Meudon spectroheliograph, 14 August 1947. Top: the Balmer series, Hα, Hβ, Hγ. Bottom: Hδ, Hϵ (in the red wing of CaII H line) and the classical CaII K3.

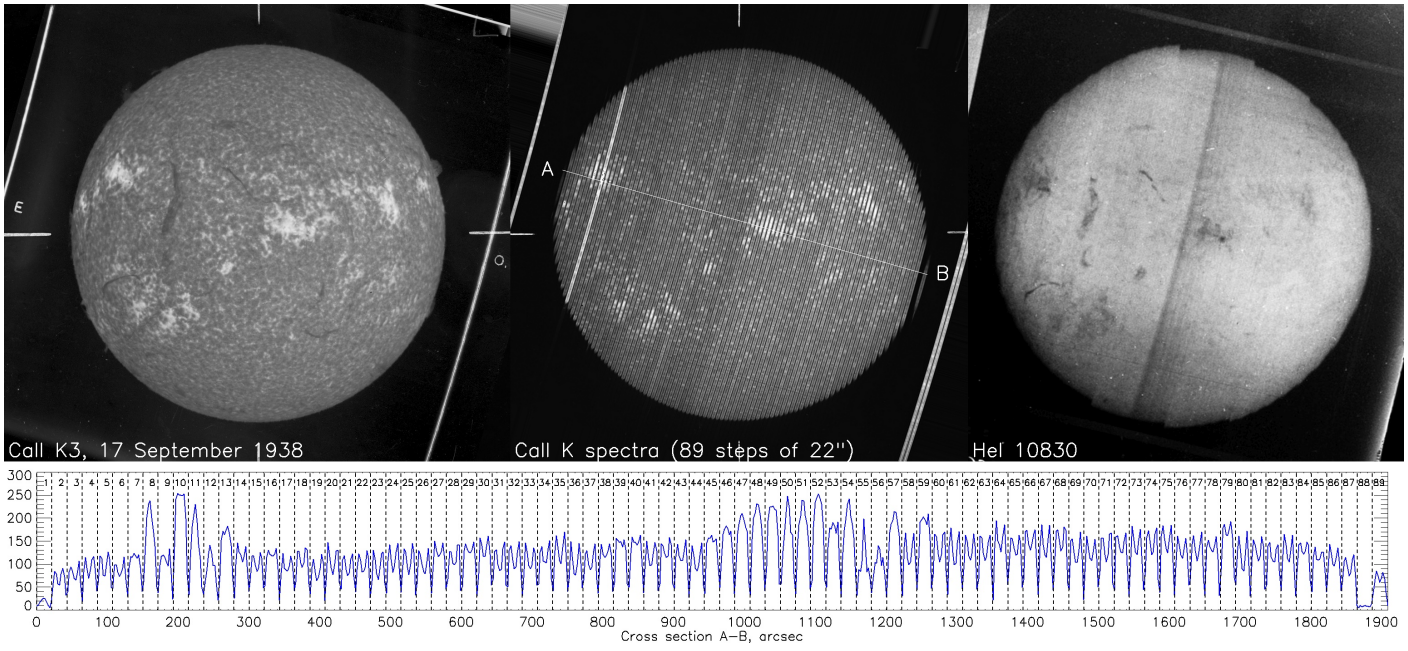

Fig. B.11. Example of the CaII K "radial velocity" collection, 17 September 1938, showing spectra recorded with a 22 arcsec step. Such spectra-images were frequently obtained from 19 April 1909 to 3 November 1943. Top: the classical CaII K3 spectroheliogram, the "radial velocity" scan of 89 slit positions across the solar disk, and the first spectroheliogram obtained worldwide in the infrared HeI 10830 Å line. Bottom: the cross section A-B shows the CaII K spectral line, step by step, for the 89 positions. The spectral range is 2.15 Å.

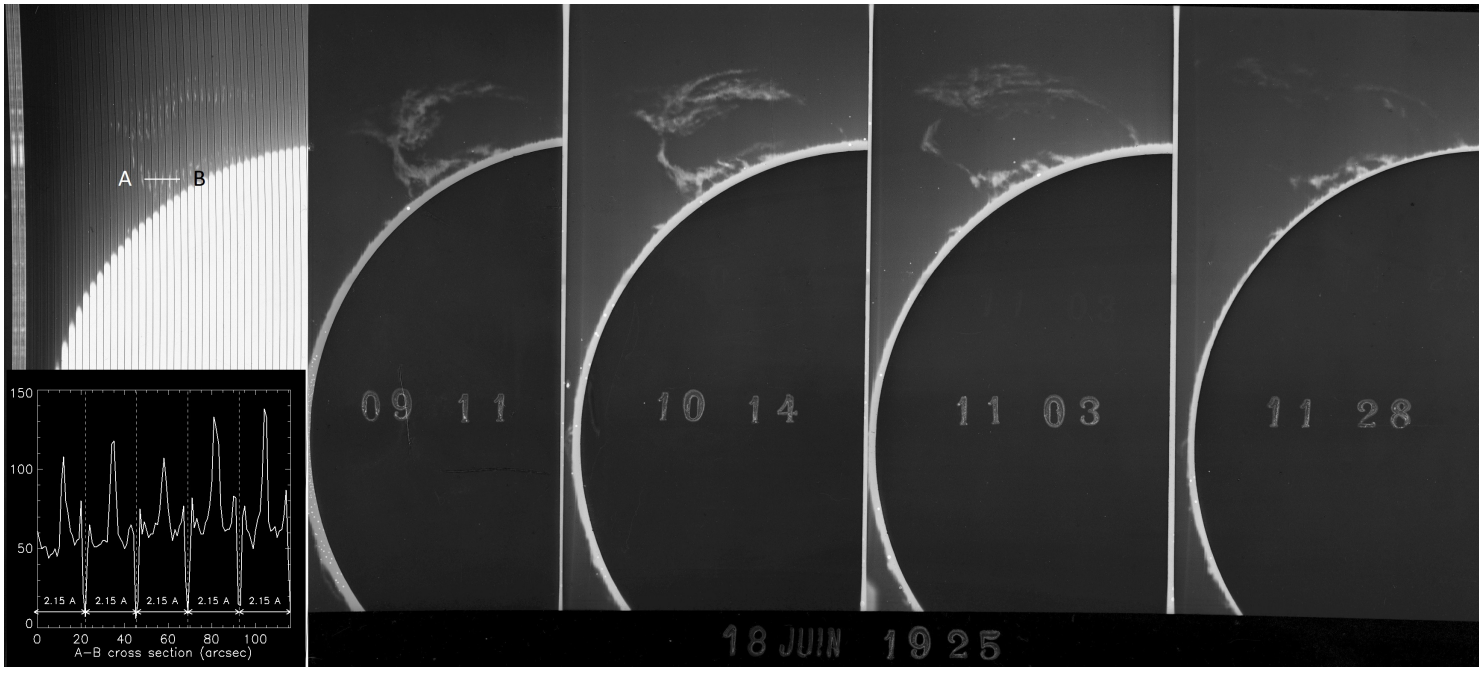

Fig. B.12. Another example of the CaII K "radial velocity" collection, the eruptive prominence of 18 June 1925. The left panel shows spectra recorded by 22 arcsec steps (2.15 Å spectral range, the disk is saturated). The five emission profiles along the cross section A-B are displayed at bottom. The other panels are the usual CaII K3 spectroheliograms recorded at 09:11, 10:14, 11:03 and 11:28 UT with an artificial moon.

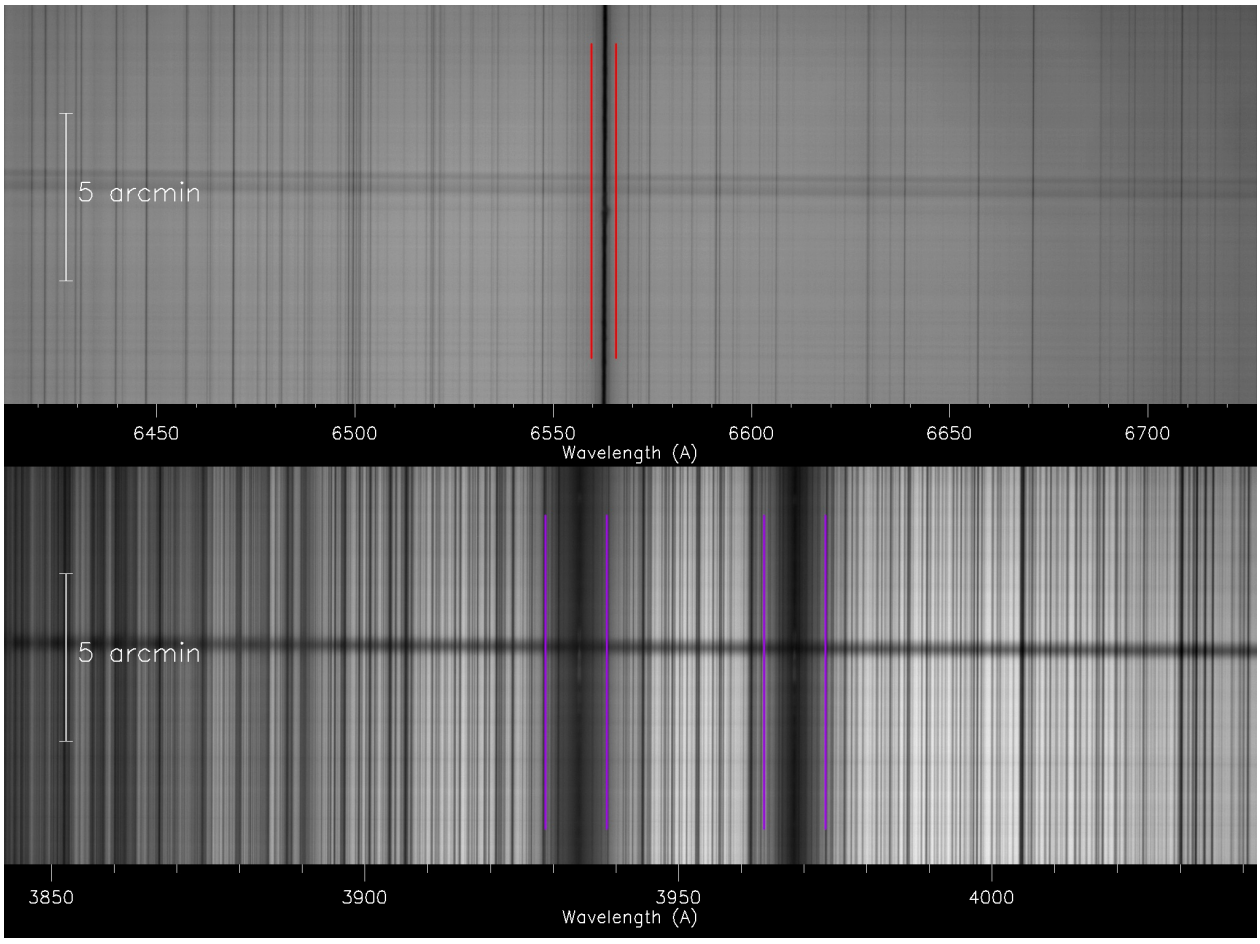

Fig. B.13. The spectral domains selected by the standard observing procedure of the 2018 version of Meudon spectroleliograph. Top: Hα, 6.2 Å spectral range, 0.155 Å/pixel (40 pixels). Bottom: CaII H and CaII K, 9.3 Å spectral range, 0.093 Å/pixel (100 pixels). Spectral ranges can be enlarged upon request with no impact on the recording time (just bigger files). A sunspot is present in the FOV.

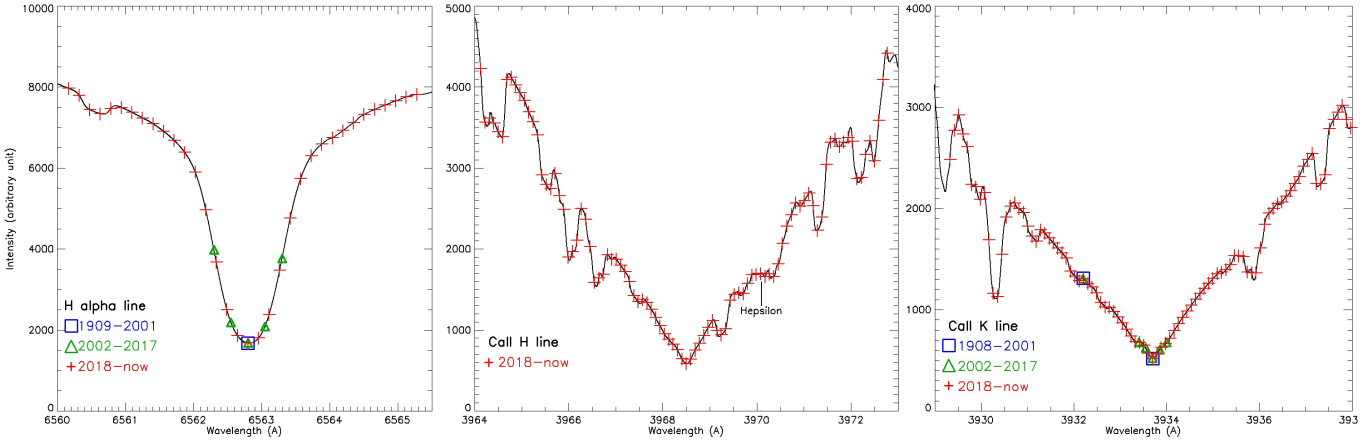

Fig. B.14. The spectra sampling in the successive versions of Meudon spectroheliograph. Left: Hα; middle: CaII H (since 2018); right: CaII K. Blue squares: observed wavelengths from 1908 to 2001 (photographic plates and films). Green triangles: CCD version from 2002 to 2017. Red crosses: sCMOS version starting in 2018. Black: atlas profiles (Delbouille et al., 1973) degraded at the spectroheliograph resolution (disk centre).

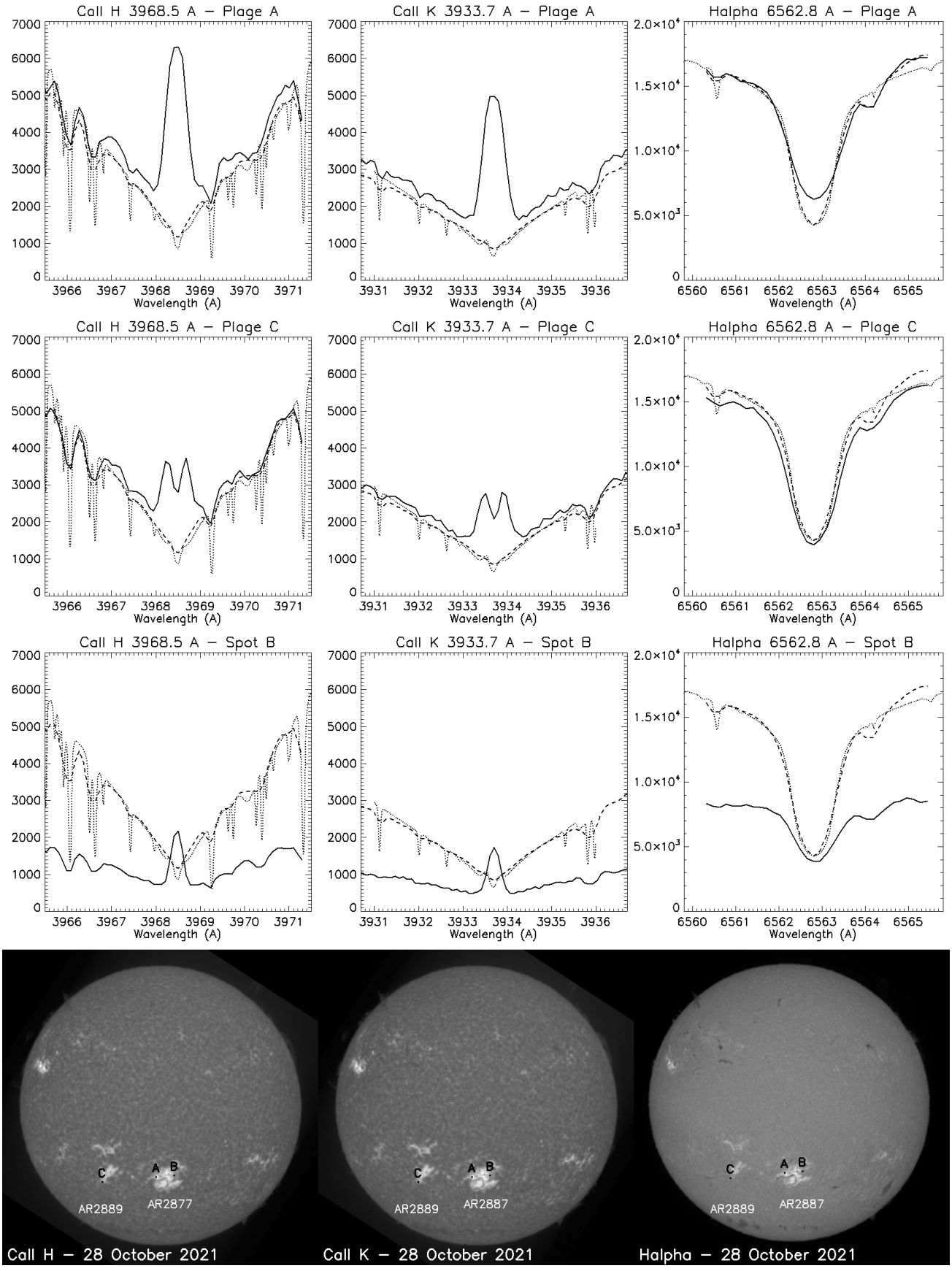

Fig. B.15. Example of line profiles provided by the 2018 version (from 3D FITS files of 28 October 2021). Column 1: CaII H (13:04 UT); column 2: CaII K (13:04 UT); column 3: Hα (13:01 UT). Row 1: bright plage A of AR2887; row 2: plage C of AR2889; row 3: sunspot B of AR2887; raw 4: CaII H, CaII K and Hα images at line centre, just before the X1.0 flare at 15:35 UT in AR2887 (southern hemisphere). Solid line: line profiles of points A, B, C; dashed line: profile of disk centre; dotted line: high resolution atlas profile of disk centre (Delbouille et al., 1973).